Journal of the Microelectronics & Packaging Society
Vol. 12, No. 1, p. 77-85. 2005

Interfacial Electrical/Dielectric Characterization in Low Temperature Polycrystalline Si

Jinha Hwang*

Dept. of Materials Science and Engineering, College of Engineering, Hongik University

Abstract: Impedance spectroscopy was applied to low temperature polycrystalline Si in order to investigate the electrical/dielectric information in polycrystalline Si. By combined microstructure and impedance spectroscopy works, it was shown that the electrical information is sensitive to the corresponding microstructure, i.e., the grain size and distribution, judged from the capacitance vs. grain size relationship. At 360 mJ/cm^2, the maximum in capacitance and the minimum in resistance correspond to the largest grain sizes of unimodal distribution in polycrystalline Si. The electrical/dielectric characterization is compared with Raman spectroscopic characterizations in terms of microstructure.

Keywords: Impedance spectroscopy, Electrical/dielectric properties, Polycrystalline, Silicon, Microstructure, Thin Film transistors

1. Introduction

Liquid crystal displays (LCDs) possess the dominant position in flat panel technologies, currently. The LCDs have been combined with amorphous Si thin film transistors. Recently, there has been significant progress in display materials and devices: low temperature polycrystalline silicon (LTPS) technology and organic electroluminescent materials[1]. LTPS transistors offer much higher mobilities ranging from 10-500cm^2/Vsec than those of the a-Si TFT ranging from 0.3-1.0cm^2/Vsec[2-4]. Higher mobilities reduce materials costs by incorporating the integration of driver ICs and reduce the display module weight and thickness. In addition, it has higher potential of a complete system on glass, including the panel ASIC, memory, photdiodes, sensors, sound chips, etc. The second organic electroluminescent materials offer higher brightness, better color characteristics, and less weight in conjunction with LTPS transistors.

However, the realization of the commercial display products faces the challenges toward mass production with high yield, requiring strict inspection and testing with a nondestructive testing tool. Among essential processes in LTPS technologies, are gate dielectrics, crystallization of amorphous Si (a-Si) into polycrystalline Si (p-Si), and ion-doping and activation. In particular, LTPS technology has been advanced based on various crystallization techniques: e.g., solid phase crystallization, excimer laser annealing, rapid thermal annealing, metal-induced crystallization, etc[5-12].

The conventional approach emphasizes the device-oriented performances rather than that focused on thin films only. The thin films are not analyzed to understand the relevant issues relating to materials only. Impedance spectroscopy has been applied successfully to electroceramics[13-17]. The frequency-dependent information has the advantages of representing different electrical/dielectric responses as distinct semi-circular arcs. Several parameters can be determined simultaneously, e.g., conductivity, dielectric constants, and the electrical homogeneities of the

*Corresponding author
E-mail: jhwang@hongik.ac.kr

constituent phases.

The microstructural features were investigated from nanoscale to submicroscale range using a variety of microscopy techniques (FESEM and TEM). The crystallinity was evaluated using Raman spectroscopy which incorporates both amorphous and polycrystalline portions simultaneously. The ramifications of the current work will be discussed in conjunction with active-matrix TFT for OLED.

2. Experimental

Amosphous Si thin films of 500Å were grown by PECVD (Plasma-Enhanced Chemical Vapor Deposition) on the SiO_2 buffer layer (of thickness 3000Å) on glass substrates, using SiH_4 and H_2 as precursors for amorphous Si. Excimer laser (the wavelength of 308 nm) was irradiated on amorphous Si thin films as a function of energy beam densities. As shown in Fig. 1, UV light is absorbed into thin films as indicated in almost no transmission, i.e., significant absorption for melting amorphous Si. Furthermore, polycrystalline Si shows the significant fraction of absorption at the wavelength of 308 nm. In crystallization processing by excimer laser, the pitch is 25 μm, the overlap is 95%, and the energy density of 210-400 mJ/cm^2. The annealing was performed under vacuum without any treatment of hydrofluoric acids on the surface of amorphous Si.

Due to high resistance of polycrystalline Si, the conventional 4-point probing can not be employed and the interdigitized lectrodes are chosen for electrical/dielectric measurements, where coplanar metal electrodes are constructed in the form of interdigitizing on the thin films by photolithography using standard lit-off techniques. The electrodes consisted of Al deposited by sputtering. The information of interdigitized electrodes is shown in Fig. 2. The resultant electrical measurements were performed using micropositioners in the probe station. The spacing between the two counterparts of the electrodes is 3 μm with the total length of 2.7m. The electrical/dielectric characteristics are performed in both alternating current and direct-current modes. The direct current voltage-current behavior was measured using a high resolution electrometer (KE 6517A, Keithley Instruments, Inc., Cleveland, OH). AC impedance spectra were obtained using impedance gain and phase analyzer (HP4194A, Hewlett Packard, Palo Alto, CA). The current-voltage char-

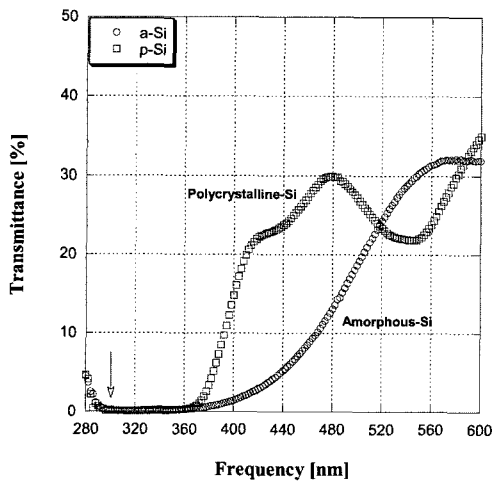

Fig. 1. Transmission vs. wavelength in amorphous Si (a-Si) and polycrystalline Si (p-Si) before and after excimer laser annealing.

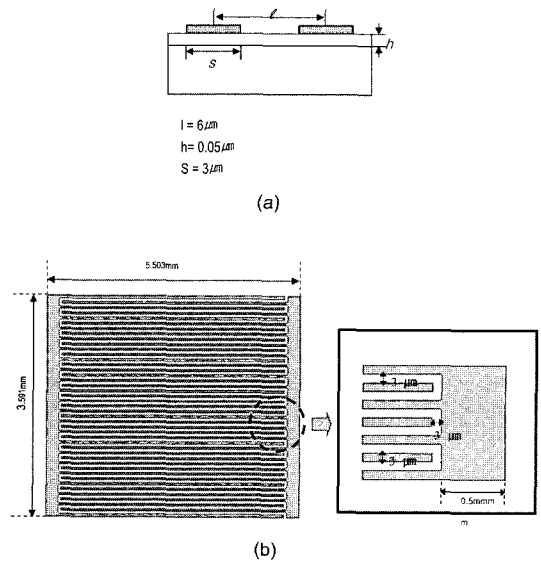

Fig. 2. Schematic of Interdigitized electroding where (a) is a side-view and (b) is a top-view.

acteristics are employed to confirm the ohmic behaviour of electroding in polycrystalline Si.

To determine the microstructure of thin films, electron microscopy techniques (SEM and TEM) were applied to p-Si. For scanning electron microscopy, the Secco etching solution is employed to clarify the microscopic features of grain boundaries in the thin films. For transmission electron microscopy, hydrofluoric acids are applied to prepare the thin films on Cu-grids since the HF solution can dissolve the silicon oxides, selectively.

3. Results and Discussion

3.1 Microstructure

Electron microscopy (SEM and TEM) were employed to determine the size and distribution of polycrystalline Si grains. Fig. 3 shows the grain size of polycrysstalline Si as a function of energy density in excimer laser annealing. Above 360 mJ/cm^2, the bimodal distributions are found. The difference between two average grain sizes increases with increasing the energy density of excimer laser annealing. Typical microstructure of uniform grains is shown in Fig. 4 and Fig. 5(a). The grains are equiaxial and quite uniform. However, the two groups of grains are distributed on polycrystalline Si in Fig. 5. Near-complete melting and complete melting occurs simultaneously, providing nucleation sites for heterogeneous crystals. Such sites are believed to cause the abnormal grain growth, leading to two modes in grain sizes. However, the average grain sizes increase with energy densities below 360 mJ/cm^2. Furthermore, SEM micrographs of Fig. 4 exhibit the equiaxial characteristics of polycrystalline Si grains. The standard deviation increases with increasing energy densities, indicating the instability of ELA above 360 mJ/cm^2.

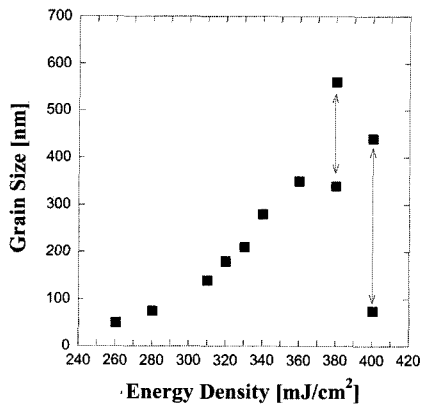

Fig. 3. Relationship between energy density vs. grain size in excimer laser annealing.

Raman spectroscopy has been applied in order to estimate the crystalline features of polycrystalline Si, in terms of peak position, full width at half maximum, and integrated intensities. (See Fig. 6) The peak position of Si has been located at 520.1cm^{-1} in a single crystalline Si wafer[18]. The peak position of polycrystalline are distributed between 516 and 517

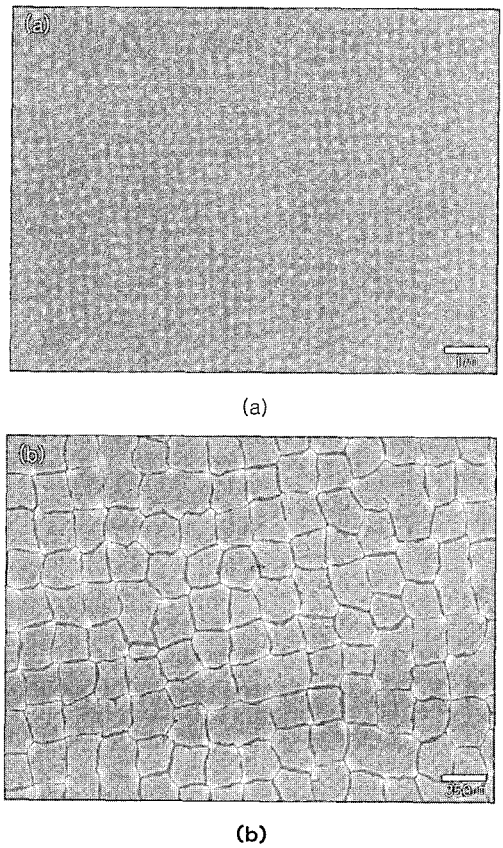

Fig. 4. Scanning electron microscopy micrographs on polycrystalline Si after Secco-etching. (a) low magnification and (b) high magnification

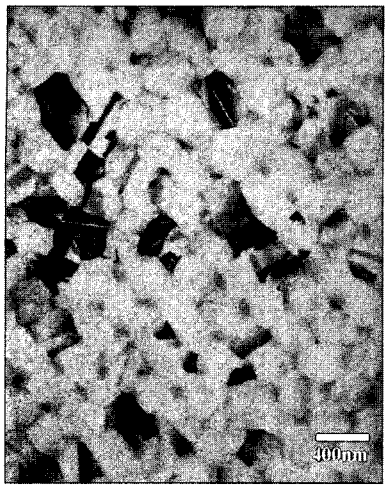

(a)

(b)

Fig. 5. Transmission electron microscopy micrograph. (a) Homogeneous Si (unimodal particle size distribution) (b) Nonuniform Si (Bimodal Pasticle size distribution).

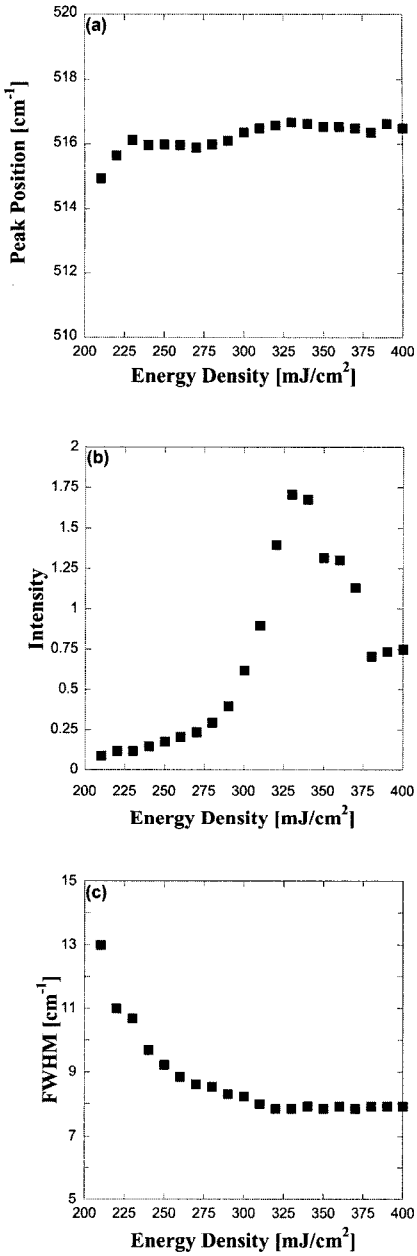

Fig. 6. Raman spectroscopic analysis in polycrystalline Si prepared using ELA. (a) Peak position vs. energy density (b) FWHM (Full Width at Half Maximum) vs. energy density (c) Intensities vs. energy density.

cm^{-1}, indicating the role of grain boundaries. The peak position did not vary significantly above 240 mJ/cm^2. The peak position is characteristic of the feature of polycrystallinity in LTPS. The grain size has a certain effect on Raman shapes below 100nm, as in Fig. 6(b). The full width at half maximum decreases with increasing the corresponding grain size, up to 100 nm. Above 100 nm, the Raman line shape appears to be independent of the grain size. The line broadening in Raman peaks are inversely proportional to the grain size, in nanoscale ranges, for less than 100nm. Also, the FWHM is larger than 7 cm^{-1} in the whole regime studied in this work. In typical Raman studies, the line widths are 1-5cm^{-1}.

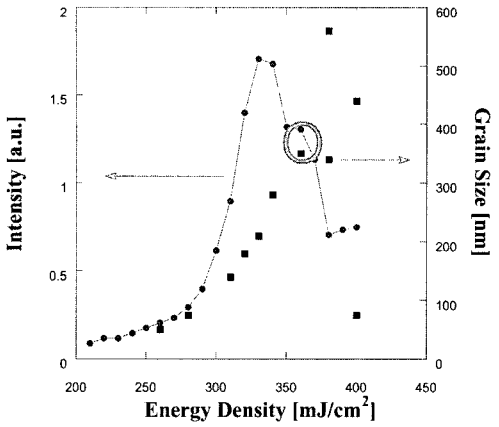

Fig. 7. Variation in Raman Intensity and grain sizes as a function of energy density.

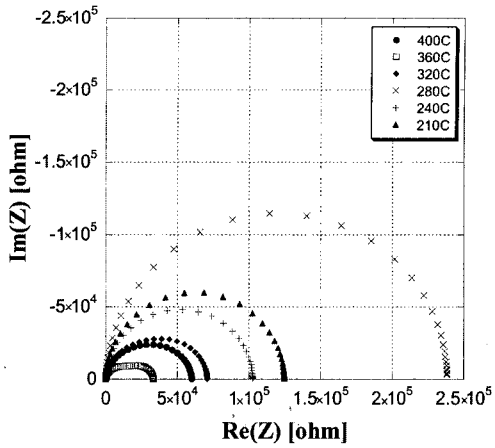

Fig. 8. Experimental Nyquist plots for polycrystalline Si a function of energy density in excimer laser annealing.

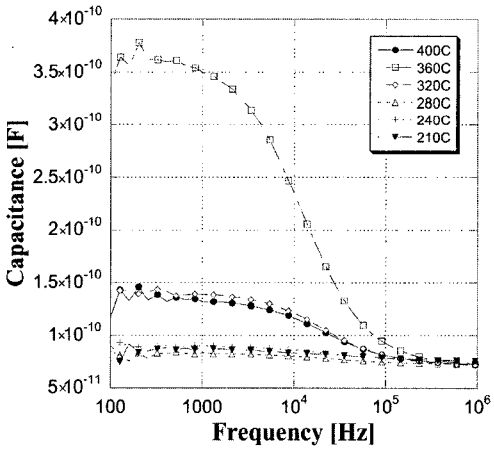

Fig. 9. Capacitance vs. frequency in various polycrystalline Si.

The difference reflects the influence of nanocrystallinity in Si crystallized using ELA. The broadening goes to maximum as the energy intensity becomes close to 200 mJ/cm^2. meaning a highest fraction of grain boundaries in polycrystalline Si.

However, the peak position of Raman Stokes line is exploited to understand the crystallinity of Si after excimer laser annealing. and the corresponding full width at half maximum (FWHM) did not change above 300mJ/cm^2. The Raman spectroscopic outputs are not in agreement with the trend in grain sizes, in peak position and FWHM's. However, the Raman intensity is more sensitive to grain growth in polycrystalline Si, as can be seen in Fig. 6(c) and Fig. 7.

3.2 Electrical and Dielectric Properties in Polycrystalline Si

IS provides the electrical/dielectric information in bulk, grain boundaries, electrodes, etc[14-17]. Depending on the time constants of bulk and interface-related responses, the bulk behavior is resolved from the interfaces. Fig. 8 shows typical impedance spectra in Nyquist plots as a function of energy density in ELA. The frequency increases from right to left. Impedance spectra of Fig. 8 can be transformed to the Bode plots, i.e., frequency vs. capacitance, as shown in Fig. 9. The variation in capacitance is found to be sensitive to the corresponding microscopic features. The current system under study can be modeled using the equivalent circuit modeling where the two parallel circuits of resistors and capacitors are connected in series. (See Fig. 10) At high frequencies, the bulk responses are dominant, while the responses due to grain boundaries control the low-frequency features in electrical/dielectric characteristics. The dielectric constant of Si is 11.7. The apparent dielectric constant confirms the electrical/dielectric responses. The total resistance is a sum of bulk resistance and resistance resulting from grain boundaries. The low-frequency capacitance increases

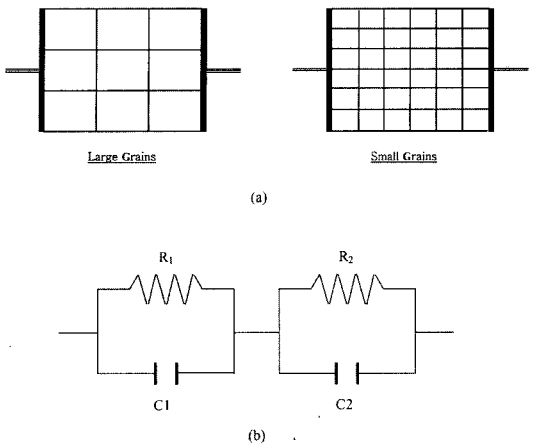

Fig. 10. (a) Schematic representation of the current system and (b) its equivalent circuit model.

and then decreases. The total resistance decreases and then increases in changing the energy densities. The critical behavior corresponds to the unusualties in microstructure. (See Fig. 11 and 12) At 360mJ/cm^2, the microstructure is characterized to be homogeneously largest in microstructure under excimer laser annealing. Fig. 13. exhibits the relation between the average grain size and capacitance (at frequencies). In general, the dielectric values increase with increasing grain sizes, as long as the distribution is homogeneous. Such behavior is described through the brick layer model. The brick layer model is routinely employed to explain the electrical properties vs. grain size in grain boundary-controlled electroceramcis. The relationship of the brick layer model is described by

$$\frac{C(gb)}{C(gi)} = \left(\frac{\varepsilon_{gb}}{\varepsilon_{gi}}\right)\left(\frac{D}{d}\right)$$

where C is the capacitance, ε is the dielectric constant, D is grain size, and d is grain boundary thickness (gb=grain boundary, and gi=grain interior). Assuming that the dielectric constants of bulk and grain boundaries are identical, the apparent capacitances are proportional to grain size, D.

As shown in Fig. 13 the capacitance at low and high frequencies are approximately in the same range. Above 100 nm (280 mJ/cm^2), the capacitance (at low frequency) is larger than that of high fre-

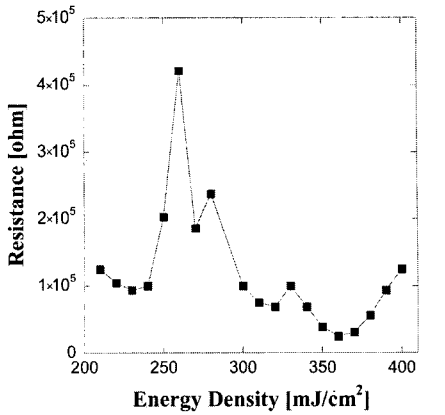

Fig. 12. Resistance vs. energy density in excimer laser annealing crystallization.

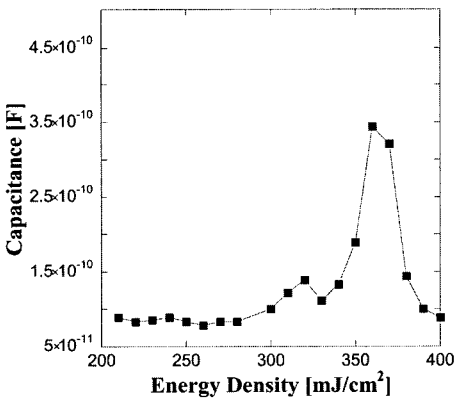

Fig. 11. Capacitance vs. energy density in excimer laser annealing crystallization.

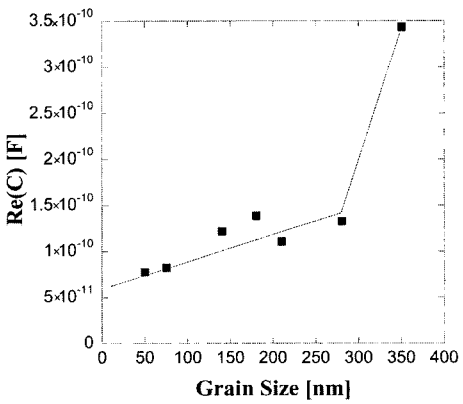

Fig. 13. Capacitance (at low frequencies) vs. average grain size.

quency, indicating that the response due to grain boundaries are significantly resolved from the bulk responses. Fig, 14 shows the fraction of grain boundaries in materials ranging from nanoscale to microscale regimes (less than 500 nm), assuming several values on grain boundary thickness ranging from 1A to 10Å. The fraction of grain boundaries are significant in the current two-dimensional microstructure as exemplified by the equiaxial microstructure in Fig. 14. In the case of 1Å, the value is approximately 4%, and the fraction of grain boundary thickness is approximately 36% in the thickness of 10Å. As in nanocrystalline electroceramics, the grain boundary feature is not so resistive rather than those of grain boundaries in microscale materials. The time constant of grain boundaries is not different from that due to bulk components, leading to a single arc without the high degree of depression in impedance Nyquist plots. As shown in impedance spectra, the shape of impedance spectra becomes singular.

The crystallization process of ELA is categorized into partial melting, near-complete melting and complete melting. In partial melting, the grain sizes increase with the energy density, found at low energy density regimes. The thickness of the melting is less than the film thickness of 500Å. At high energy density regimes, the whole thin film of amorphous Si are melted, reamorphizes and grain size decreases with increasing the energy density. In between the partial melting and the complete melting, the melting thickness is approximate to the thickness of a-Si. The later growth occurs significantly, called as the near-complete melting. In optimum conditions, grain sizes can reach several microns wide. From the current work of microstructure as shown in Fig. 3, the complete melting seems to occur at equal to or larger than 380mJ/cm^2 and the partial melting appears to be located below 350 mJ/cm^2. Between 350 and 370 mJ/cm^2, the near-complete melting takes place. The bimodal distribution of grain sizes are considered as an indirect evidence of complete melting where the nucleation rate for grain growth is high, leading to the small grain sizes.

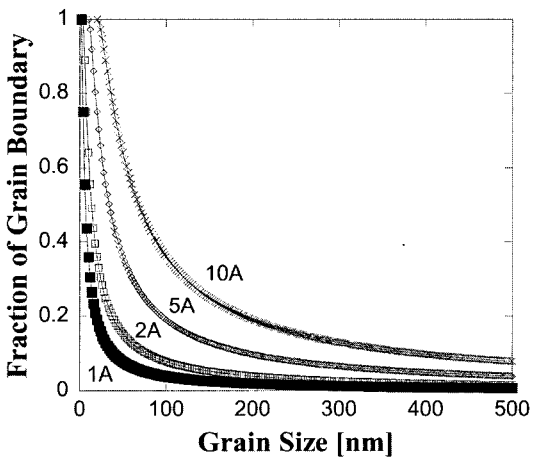

Fig. 14. Relative fraction of grain boundary in polycrystalline Si (assuming the grain boundary thickness of 1Å, 2Å, 5Å, and 10Å)

Crystallinity of polycrystalline Si affects the mobilities of charge carriers, determining the subthreshold slope, leakage currents, and stabilities in TFT devices[19]. The current work provides the effective large grain size for TFT performances, where the critical values in electrical properties are found: maximum in capacitance and minimum in resistance. Below the optimum points, the number of grain boundaries increasing with decreasing grain sizes, leading to the increase in the apparent resistance and the decrease in the apparent capacitance. Above the critical grain size, the bimodal distribution of grain sizes are found, i.e., a mixture of large and small grains result to the increase in total grain boundary fractions, also the increase in resistance, where the microscopic schematic is a mixture of Fig. 10(a). In the mixture, the number of grain boundaries is larger than that of the largest grained structure (in this work, at 360 mJ/cm^2) In terms of capacitance, the capacitance at low frequency are dependent upon the behavior in grains size and the distributions. In flat panel LTPS industries, the quality of polycrystalline Si is estimated after the TFT structure is fabricated through tens of processing steps involving numerous photolithographic works. The report provides a simplified tool which can eval-

uate the quality of polycrystalline Si, with simplified processing and structure only with one photolithographic mask. The introduction of this technique can be standardized in combination with the TFT characteristics, contributing to the strict control of TFT performance. The highly-controlled TFT can be connected to organic light-emitting diodes operating in the mode of active matrix driving scheme.

4. Conclusions

From the study on the grain size distribution of polycrystalline Si, the largest grain size was found at 360 mJ/cm^2, keeping the unimodal distribution of grain sizes. The maximum grain size reached the values of approximately 380mJ/cm^2, of the bimodal distribution in grain sizes. The crysatllinity of polycrystalline Si was investigated using Raman spectroscopy where the Raman intensity is more sensitive to the variation in microstructural feature, i.e., grain size compared to those of the peak position and the peak width at half maximum. Impedance spectroscopy was applied to investigate the electrical/dielectric properties of low temperature polycrystalline Si as a function of energy density. At 360mJ/cm^2, the largest grain size exhibited the minimum in resistance and maximum. In particular, the capacitance varied with regard to the corresponding microstructure. The bimodal distribution of grain sizes was found beginning with 380 mJ/cm^2. In summary, the impedance spectroscopy is proven to be an effective tool for investigating the microstructure in polycrystalline Si.

Acknowledgements

This work was supported by the Korea Research Foundation Grant (KRF-2002-003-D00157).

References

1. N. Komiya, R. Nishikawa, M. Okuyama, T. Yamada, Y. Saito, S. Oima, K. Yoneda, H. Kanno, H. Takahashi, G. Rajeswaran, M. Itoh, M. Boroson, and T. K. Hatear, "Active Matrix OLED Displays with Low-Temperature Poly-Si TFT," Proceeding of the 10th International Workshop on Inorganic and Organic Electroluminescence, 347 (2000).
2. K. Sera, F. Okumura, H. Uchida, S. Itoh, S. Karelso, and K. Hotta, "High-Performance TFT's Fabricated by XeCl Excimer Laser Annealing of Hydrogenated Amorphous-Silicon Films," IEEE Trans. ELectron Devices 36[12] 2868 (1999).
3. M.A. Crowder, P.G. Garey, P.M. Smith, R.S. Sposili, H.S. Cho, and J.S. Im, "Low-TemperatuSingle Crystal Si TFT's Fabricated on Si Films Processed via Sequential Lateral Solidification," IEEE Electron Device Lett. 19[8] 306 (1998).
4. M. Yamamoto, H. Nishitani, M. Sakai, M. Gotoh, Y. Taketomi, T. Tsutsu, and M. Nishitani, High Performance Low Temperature Poly-Si TFT Obtained by a New Fabrication Method," Euro Display 99 Proceedings p.53 (1999).
5. E. Ibok and S. Garg J, "A Characterization of the Effect of Deposition Temperature on Polysilicon Properties," Electrochem. Soc. 140 2927 (1993).
6. S.W. Lee and S.K. Joo, "Low Temperature Poly Si Thin Film Transistor Fabrication by Metal-Induced Lateral Crystallization," IEEE Electron Device Lett. 17 160 (1996).
7. S.Y. Lee, Y.C. Jeon, and S.K. Joo, "Pd Induced Lateral Crystallization of Amorphous Si Thin Films," Appl. Phys. Lett. 66[13] 1671 (1995).
8. J.S. Im and R.S. Sposili, "Crystalline Si Films for Integrated Active-Matrix Liquid Crystal Displays," Mat. Res. Bull. 2[3] 39 (1996).
9. J.-B. Lee, C.-J. Lee, and D.-K. Choi, "Influence of Various Elements on Field-Aided Lateral Crystallization of a-Si Film," Jpn. J. Appl. Phys. 40 6177 (2001).
10. A.R. Song, A Study on The Solid Phase Crystallization of LPCVD a-Si Thin Films by Alternating Magnetic Flux. M.S. Thesis, Hongik University (2000).
11. R. Kakkad, J. Smith, W. S. Lau, S. J. Fonash, and R. Kerns, "Crystallized Si Films by Low-Temperature Rapid Thermal Annealing of Amorphous Silicon," J. Appl. Phys. 65 2069 (1989).
12. K.-C. Park, I.-H. Song, S.-H. Jung, J.-W. Park, and M.-K. Han, "The Composite Effects of MILC and ELA on the Crystallization of a-Si Film," AM-LCD 2000, 147 (2000).
13. G.W. Farrell, I.A. Cermak, P. Silvester, and S. K. Wong, "Capacitance and Field Distributions for Interdigital Surface-Wave Transducers," IEEE Trans. Sonics Ultrason SU-17[3] 188 (1970).

14 I.M. Hodge, M.D. Ingram, and A.R. West, "Impedance and Modulus Spectroscopy of Polycrystalline Electrolytes," J. Electroanal. Chem. 74 125 (1976).
15. J.T.S Irvine, D.C. Sinclair, and A.R. West, "Electroceramics: Characterization by Impedance Spectroscopy," Adv. Mater. 2[3] 132 (1993).
16. J.T.S. Irvine, A. Huanosta, R. Valenzuela, and A.R. West, "Electrical Properties of Polycrystalline Nickel Zinc Ferrites," J. Am. Ceram. Soc. 73[3] 729 (1989).
17. R.S. MacDonald, Impedance Spectroscopy, John Wiley Sons Inc. (1987).
18. T. Inushima, N. Kusumoto, N. Kubo, and H.-Y. Zhang, and S. Yamazaki, "Phase Transformation in Amorphous Silicon Under Excimer Laser Annealing Studied by Raman Spectroscopy and Mobility Measurements," J. Appl. phys. 79[12] 9064 (1996).
19. S. Uchikoga, "Low-Temperature Polycrystalline Silicon Thin-Film Transistor Technologies for System-on-Glass Displays," MRS Bulletion, 881 (2002).